Supporting Information

Chemisorption of Atomically Precise 42-Carbon Graphene Quantum Dots on Metal Oxide Films Greatly Accelerates Interfacial Electron Transfer

Peng Han[1], Ian Cheng-Yi Hou[1], Hao Lu[1], Xiao-Ye Wang[1], Klaus Müllen[1,2], Mischa Bonn[1], Akimitsu Narita[1,3], Enrique Cánovas[1,4,*]

[1] Max Planck Institute for Polymer Research, Ackermannweg 10, 55128 Mainz, Germany.
[2] Institute of Physical Chemistry, Johannes Gutenberg University Mainz, Duesbergweg 10-14, 55128 Mainz, Germany.
[3] Organic and Carbon Nanomaterials Unit, Okinawa Institute of Science and Technology Graduate University, Okinawa 904-0495, Japan.
[4] Instituto Madrileño de Estudios Avanzados en Nanociencia (IMDEA Nanociencia), Faraday 9, 28049 Madrid, Spain.

** Correspondence to: enrique.canovas@imdea.org*

Table of Contents **Page**

MATERIALS AND METHODS

General methods

All reactions working with air- or moisture-sensitive compounds were carried out under argon atmosphere using standard Schlenk line techniques. Unless otherwise noted, all starting materials and reagents were purchased from commercial sources (such as Alfa Aesar, Sigma-Aldrich, Acros and TCI) and used without further purification. Thin layer chromatography (TLC) was performed on silica gel coated aluminum sheets with F254 indicator and silica gel column chromatography separation was performed with the 0.063–0.200 mm particle size. Nuclear Magnetic Resonance (NMR) spectra were recorded in deuterated solvents using Bruker AVANCE III 500 and Bruker AVANCE III 700 MHz NMR spectrometers. Chemical shifts (δ) were expressed in ppm relative to the residual of solvent (CD2Cl2 @ 5.32 ppm for 1H NMR, 54.00 ppm for 13C NMR, C2D2Cl4 @ 6.00 ppm for 1H NMR, 73.78 ppm for 13C NMR). Coupling constants (*J*) were recorded in Hertz (Hz) with multiplicities explained by the following abbreviations: s = singlet, d = doublet, t = triplet, q =quartet, dd = double of doublets, dt = doublet of triplets, m = multiplet, br = broad. The micro-FT-IR spectra were recorded through a diamond anvil cell (transmission mode) with a Nicolet Nexus FT-IR spectrometer coupled with a Thermo Electron Continuμm IR microscope. The wavenumber (ν) is expressed in cm^{-1}. UV–vis absorption spectra were measured on a Perkin-Elmer Lambda 900 spectrophotometer at room temperature. High-resolution mass spectra (HRMS) were recorded by matrix-assisted laser decomposition/ionization (MALDI) using 7,7,8,8-tetracyanoquinodimethane (TCNQ) as matrix on a Bruker Reflex II-TOF spectrometer (MALDI-TOF HRMS).

Sample preparation

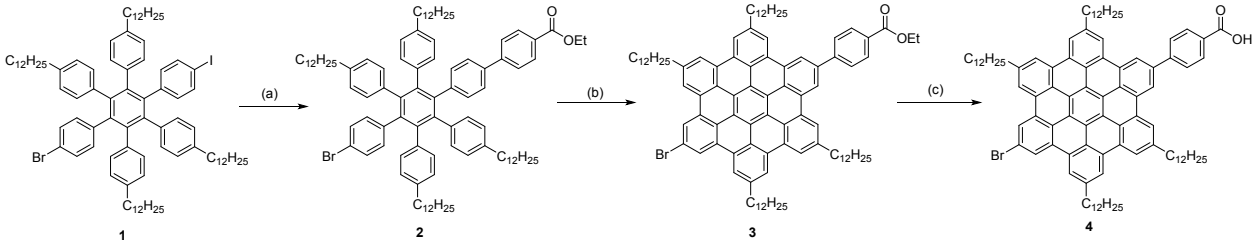

Scheme S1. The synthesis of GQD_{c42}-PhCOOH. Reagents and conditions: (a) $Pd(PPh_3)_4$, K_2CO_3, toluene/water/ethanol, 70 °C, 1 h. (b) $FeCl_3$, dichloromethane/nitromethane, rt, 1 h. (c) KO*t*Bu, H_2O (3 eq.), tetrahydrofuran, rt, overnight.

Synthesis of ethyl 5'-(4-bromophenyl)-4-dodecyl-3',4',6'-tris(4-dodecylphenyl)-[1,1':2',1'':4'',1'''-quaterphenyl]-4'''-carboxylate (2 in scheme S1)

To a suspension of 4-bromo-4''-dodecyl-3',5',6'-tris(4-dodecylphenyl)-4'-(4-iodophenyl)-1,1':2',1''-terphenyl[3] (0.18 g, 0.12 mmol) and 4-ethoxycarbonylphenylboronic acid (77 mg, 0.40 mmol) in toluene (5 mL) was added a solution of K_2CO_3 (0.9 g, 7 mmol) in water (1 mL) and ethanol (1 mL). This mixture was degassed by freeze-pump-thaw technique (1 cycle). $Pd(PPh_3)_4$ (15 mg, 0.013 mmol) was then added to the mixture, which was further degassed by freeze-pump-thaw technique for another 2 cycles. The mixture was then heated at 70 °C under vigorous stirring and monitored by TLC until the starting material was consumed (about 1 h). After cooling to a room temperature, the mixture was diluted with diethyl ether and washed with water and brine. The organic layer was then dried over $MgSO_4$ and the solvent was removed in vacuo. The residue was purified by silica gel column chromatography (eluent: ethyl acetate/hexane = 1/6) to afford the title compound as pale yellow oil (0.14 g, 81%). ^{1}H NMR (700 MHz, CD_2Cl_2): δ 7.98 (d, J = 8.4 Hz, 2H), 7.49 (d, J = 8.4 Hz, 2H), 7.17 (d, J = 8.1 Hz, 2H), 6.98 (d, J = 8.4 Hz, 2H), 6.93 (d, J = 8.1 Hz, 2H), 6.76–6.69 (m, 14 H) 6.67 (d, J = 8.0 Hz, 4H), 4.33 (q, J = 7.1 Hz, 2H), 2.39 (t, J = 7.5 Hz, 4H), 2.35 (t, J = 7.5 Hz, 4H), 1.41 (quint, J = 7.9 Hz, 8H), 1.39–1.02 (m, 75 H), 0.92–0.85 (m, 12 H). ^{13}C NMR (126 MHz, CD_2Cl_2) δ 166.78, 145.49, 141.85, 141.06, 140.91, 140.86, 140.69, 140.50, 140.41, 139.84, 138.42, 138.32, 136.77, 133.81, 132.67, 131.78, 131.76, 130.34, 130.10, 129.61, 127.34, 127.26, 126.99, 125.66, 119.64, 61.41, 54.43, 54.22, 54.00, 53.79, 53.57, 35.81, 32.52, 31.84, 31.80, 30.34, 30.30, 30.27, 30.20, 30.10, 30.04, 29.97, 29.95, 29.39, 29.36, 23.28, 14.68, 14.46. HRMS (MALDI-TOF) calcd. for $C_{99}H_{133}BrO_2$ $[M]^+$, 1432.9489. Found $[M]^+$ 1432.9426.

Synthesis of ethyl 4-(11-bromo-5,8,14,17-tetradodecylhexa-*peri*-hexabenzocoronen-2-yl)benzoate (3 in scheme S1)

A solution of **2** (0.17 g, 0.12 mmol) in unstabilized dichloromethane (50 mL) was degassed by argon bubbling for 5 min. The argon bubbling was continued for the whole reaction period. To this solution was added a solution of $FeCl_3$ (0.6 g, 4 mmol) in nitromethane (5 mL). The reaction mixture turned dark brawn immediately. The mixture was stirred at a room temperature for 1 h and then poured into methanol (400 mL). Two drops of brine was added to the mixture to facilitate precipitation. The precipitates were collected by vacuum filtration and purified by silica gel column chromatography (eluent: hot toluene) to afford the title compound as a bright yellow solid (161 mg, 95%). ^{1}H NMR (700 MHz, $C_2D_2Cl_4$, 373 K): δ 8.37 (d, J = 7.0 Hz, 2H), 8.17 (br, 2H), 7.92 (d, J = 7.0 Hz, 2H), 7.83 (br, 2H), 7.77 (br, 2H), 7.63 (br, 2H), 7.60 (br, 2H), 7.49 (br, 2H), 4.60 (q, J = 7.2 Hz, 2H), 2.78 (br, 4H), 2.70 (br, 4H), 1.90 (br, 4H), 1.83 (br, 4H), 1.73-1.18 (m, 75H), 1.02-0.87 (m, 12H). ^{13}C NMR (176 MHz, $C_2D_2Cl_4$, 373 K): δ 166.25, 145.96, 139.03, 138.99, 135.37, 135.25, 135.21, 130.25, 130.10, 129.46, 128.97, 128.19, 128.15, 127.03, 123.01, 122.58, 121.72, 121.70, 121.53, 121.47, 120.86, 120.52, 120.25, 120.04, 118.62, 118.00, 117.60, 117.48, 117.28, 60.79, 36.77, 36.67, 31.72, 31.56, 31.46, 29.95, 29.77, 29.74, 29.66, 29.63, 29.52, 29.14, 22.41,

14.33, 13.74. IR: ν = 3063, 2952, 2917, 2849, 1719, 1609, 1576, 1466, 1271, 1104, 1021, 861, 849, 771, 721, 705. HRMS (MALDI-TOF) calcd. for $C_{99}H_{121}BrO_2$ $[M]^+$, 1420.8550. Found $[M]^+$ 1420.8501.

Synthesis of 4-(11-bromo-5,8,14,17- tetradodecylhexa-*peri*-hexabenzocoronen -2-yl)benzoic acid (4 in scheme S1)

To a solution of **3** (30 mg, 21 μmol) and water (1.1 mg, 62 μmol) in tetrahydrofuran (7 mL) was added a tetrahydrofuran solution of KO*t*Bu (0.19 mL, 1 M, 190 μmol) at a room temperature. The mixture was stirred overnight and poured into methanol (50 mL). The precipitates were collected by vacuum filtration and washed with water, methanol and acetone to afford the title compound as a brownish orange solid (29 mg, 99%). HRMS (MALDI-TOF) calcd. for $C_{97}H_{117}BrO_2$ $[M]^+$, 1392.8237. Found $[M]^+$ 1392.8180. IR: ν = 3062, 2952, 2919, 2849, 1687, 1609, 1576, 1464, 1414, 1367, 1181, 861, 849, 774, 719, 613, 553, 492. Because of the strong aggregation of **3** in solution, NMR spectra could not be resolved.

Preparation of GQDs sensitized metal oxide films

Mesoporous metal oxide films (SnO_2, ZnO, TiO_2) were prepared by doctor-blading method. After sintering at 450 °C for 2h, they were left to cool down to 80 °C. After this, we immersed the mesoporous films in an anhydrous toluene solution containing the graphene dots (1 mg/5 mL). To allow the sensitization, the samples remained in a N_2 purged glovebox overnight. The obtained sensitized films were rinsed in Toluene and dried under N_2 environment without applying any thermal treatment during the process.

Optical Pump-THz Probe (OPTP) Spectroscopy

The detailed working principle of OPTP spectroscopy has been introduced elsewhere[1]. A Ti:sapphire amplified laser system (Spitfire ACE by Spectra-Physics) producing ultra-short laser pulses of ~40 fs duration at 800 nm at 1 kHz repetition rate was used to drive our OPTP set-up. About ~ 900 mW energy is used to run the optical pump-THz probe spectrometer setup. For the THz generation and detection, 10% of the incoming laser beam is used (90 mW). THz radiation is generated in a phase-matched manner by optical rectification in a ZnTe crystal (<110> orientation, 10×10×1 mm thickness, purchased from MaTeck). The ZnTe generation crystal is pumped with a slightly focused beam (~ 3 mm diameter) of 800 nm light (80 mW power, 50 fs FWHM). The THz light exits the ZnTe generation crystal slightly divergent and is first collimated and subsequently focused on the sample using a pair of off-axis parabolic mirrors. The transmitted THz pulses are recollimated and focused on a second ZnTe detection crystal by another pair of parabolic mirrors, where the instantaneous THz field strength is detected through electro-optical sampling. In our

experiment, graphene quantum dots were selectively excited by a 400nm optical pulse which was generated by frequency doubling of the fundamental 800 nm in a BBO crystal. Assuming thin film approximation applies and fixing the arriving time of sampling beam at the THz peak, the magnitude of the real part of photoconductivity as a function of pump-probe time delay (up to 1 ns for our setup) was provided. This measurement gives information about the product of the photo-induced charge carrier density and their average mobility. To deconvolute these two factors and interrogate the nature of interfacial ET frequency-resolved photoconductivity needs to be measured. In this measurement, the recorded photo-induced change in amplitude and phase of the propagating THz pulses yield information on, respectively, the real and imaginary parts of the complex-valued photoconductivity of the sample under study.

Ultraviolet Photoelectron Spectroscopy (UPS), Valence Band X-ray Photoelectron Spectroscopy (VBXPS) , and X-ray Photoelectron Spectroscopy (XPS)

UPS and VBXPS measurements were conducted on a Kratos Axis Ultra^{DLD} spectrometer (Kratos, Manchester, England). In these measurements, the samples were transported from an inert-atmosphere glovebox (<1 ppm of O_2) to the vacuum system (2×10^{-7} mbar) immediately after they were prepared. In UPS measurement, electrical contact was always applied. The sample was held at a bias of –9 V with respect to the spectrometer. Illumination at 21.2 eV is provided by the He(I) emission line from a helium discharge lamp, and the chamber pressure increases from ~10^{-10} to ~10^{-7} mbar. Photoelectron emission was collected at 0° from the surface normal of the samples. The spectra were taken in three different spots to confirm the spectra reproducibility and irradiation exposure time was kept under one minute. VBXPS spectra were collected using an Al Kα excitation source with a photon energy of 1487 eV. Spectra were acquired in hybrid mode of the analyzer lens, using a 0° take-off angle, which is defined as the angle between the surface normal and the axis of the analyzer lens.

First-Principles Calculations

DFT calculations were performed using the Gaussian 09 software package.[2] The geometry and energies were calculated at the B3LYP/6-311+G(d,p) level. All alkyl chains were replaced with methyl groups for computational simplicity.

SUPPLEMENTARY FIGURES

OPTP dynamics of GQDs Sensitized SnO_2 in Linear Single-Exciton Regime

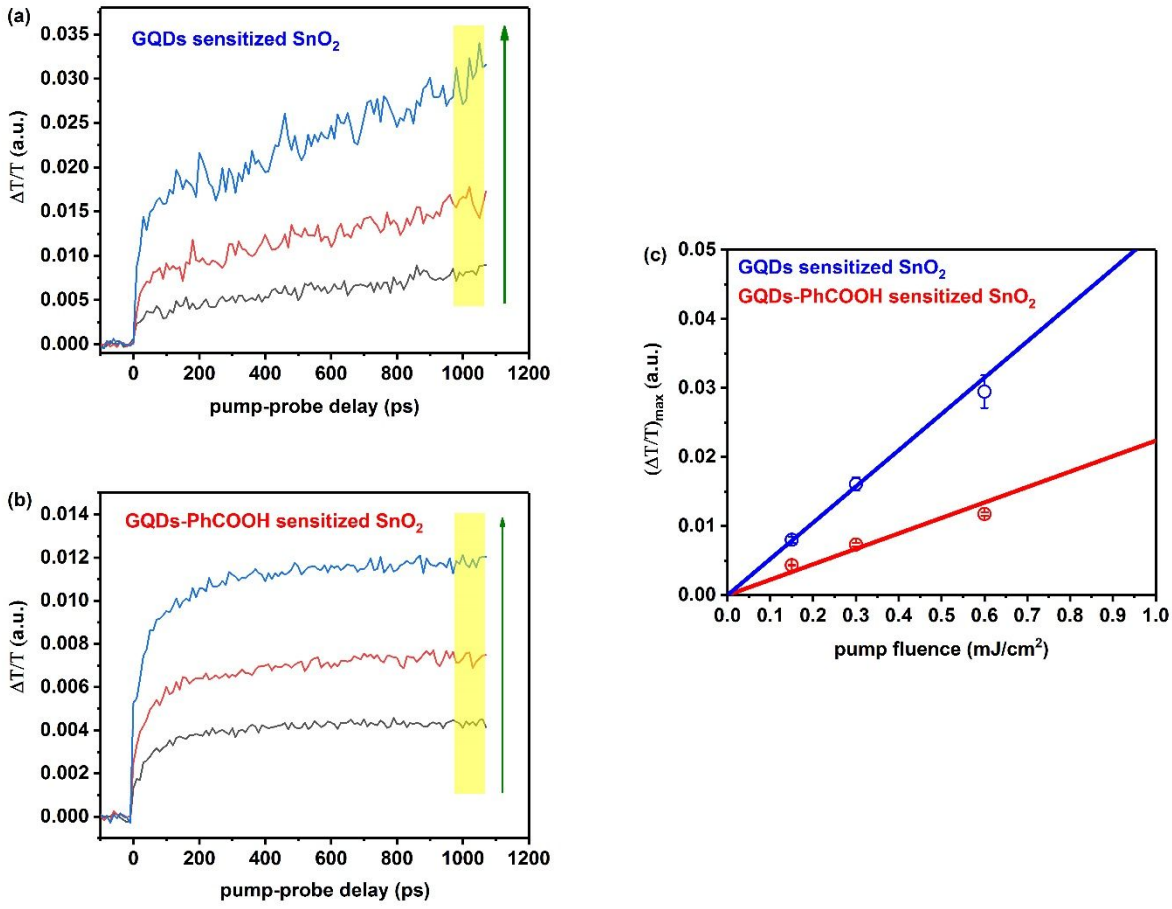

Figure S1. OPTP dynamics of (a) GQDs sensitized SnO_2 and (b) GQDs-PhCOOH sensitized SnO_2 as a function of 400 nm pump excitation fluence. The data demonstrate that excitation in the linear regime (i.e., the signals scale linearly with fluence, hence no change of oxide mobility in the oxide is resolved).

Oscillations in frequency-resolved photoconductivity spectra

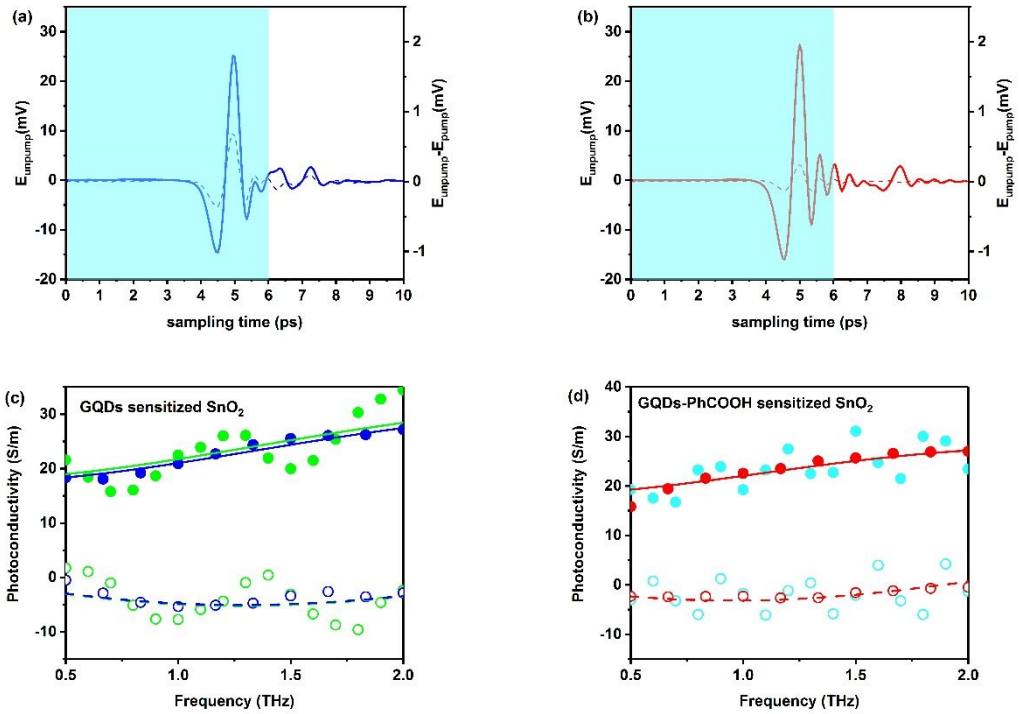

Figure S2. (Top figures) THz probe line shapes in the time domain for both samples. A series of oscillations appear at time delays above 6 ps that we tentatively correlate with multiple reflections of the pump excitation for our sample/substrate geometry (QD-oxide film/fused silica). Fourier transformation of bare data reveals oscillations in the complex conductivity line shape in the frequency domain (bottom panels). The oscillations can be filtered out by shorting the time spam (from 0 to 6ps) prior Fourier transformation. Fits to the Drude-Smith model for bare and filtered data in the frequency domain (solid and dashed lines in bottom panel) demonstrate that the filtering protocol is barely affecting the inferred photophysical response of the analyzed systems.

OPTP dynamics of GQDs Sensitized ZnO/TiO_2

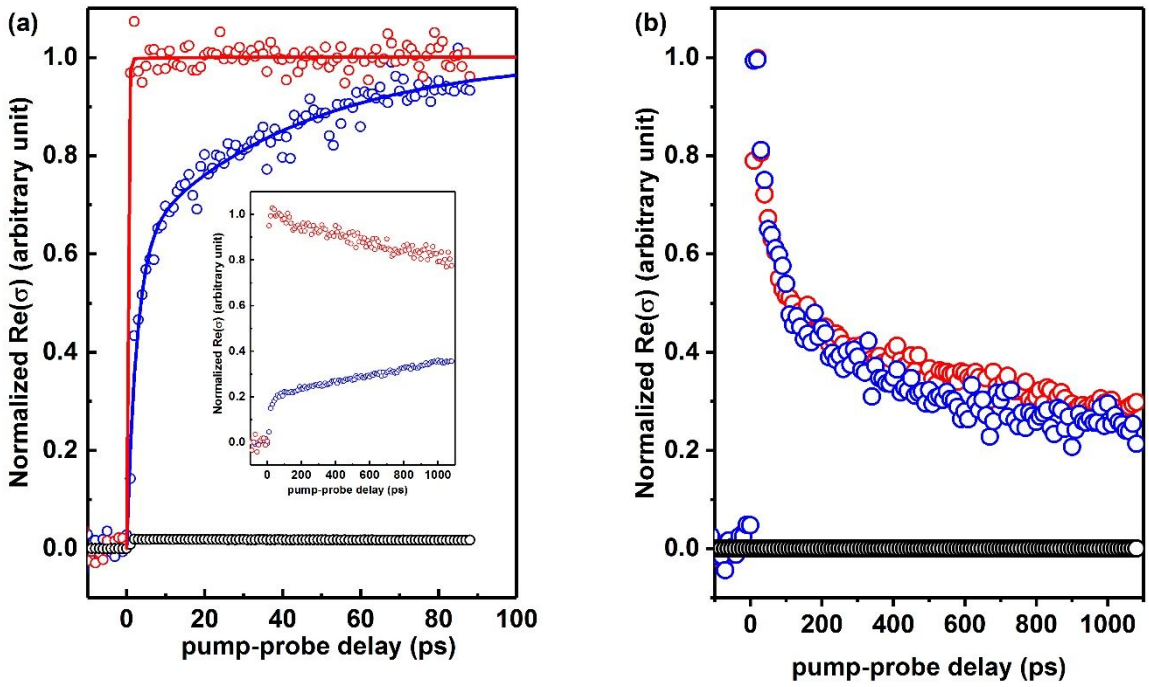

Figure S3. Normalized OPTP dynamics of GQDs sensitized ZnO films (a) and TiO_2 films (b) excited under the same conditions employed for sensitized SnO_2 films for fig 2a in the manuscript. Dynamics in bare ZnO and TiO_2 films are also shown (black open circles). Biphasic fits for the ZnO case provide ET time constant τ_1 = 3 ps, τ_2 = 42 ps for physisorbed case and τ_1 = 0.3 ps, τ_2 = 13 ps for chemisorbed case respectively. The ET components for TiO_2 are faster than our setup resolution (sub 100fs).

Frequency-Resolved Photoconductivity of GQDs Sensitized ZnO/TiO_2

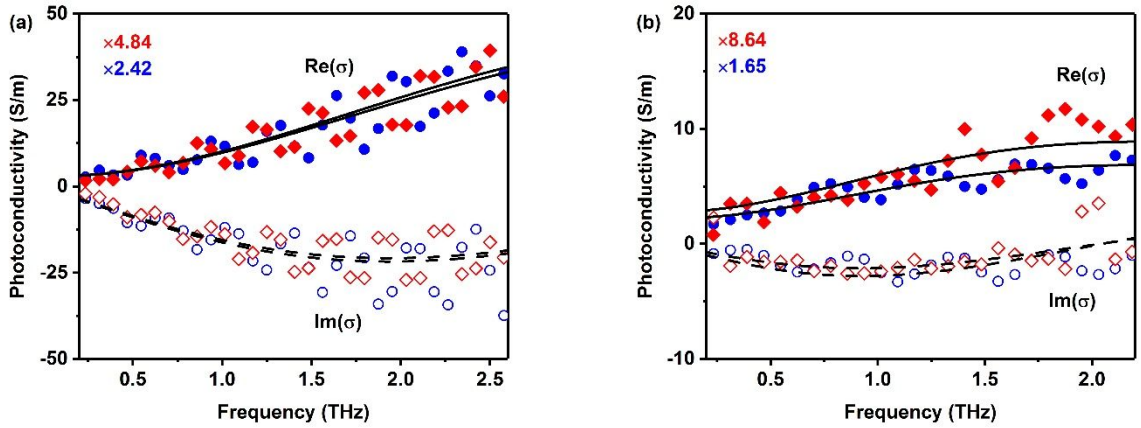

Figure S4. Frequency-resolved complex photoconductivity (solid and open dots for the real and imaginary components) for (a) sensitized ZnO systems and (b) TiO_2 system (1ns after excitation). Solid and dashed lines are best fits to the DS model. Best fit in mesoporous ZnO films provides a scattering rate and localization parameter of τ_s = 33.6 fs and c = -0.97, which agrees well with previous reports [3]. For titania, we obtain from the DS fits τ_s = 64.5 fs and c = -0.84, also in agreement with literature[4].

UPS data of Mesoporous SnO_2 Film

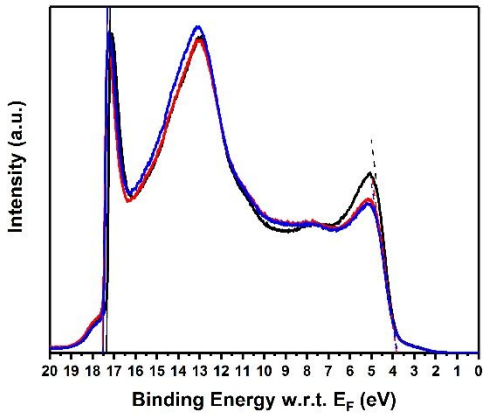

Figure S5. Ultraviolet photoelectron spectroscopy (UPS) data of three spots on the same SnO_2 film (solid lines). Two cutoffs were resolved for each spectrum: the one close to the Fermi level representing valence band edge (VBE) of SnO_2; the one far from the Fermi level representing vacuum level in each spot. From these cutoffs, we can obtain the workfunction of the system.

Fig.S6. Absorption Spectrum of Mesoporous SnO_2 Film

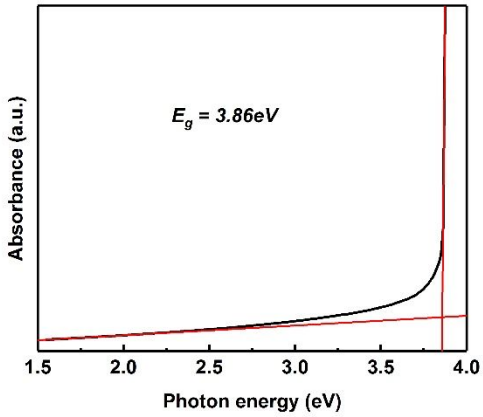

Figure S6. Absorption spectrum of bare SnO_2 film. A bandgap of 3.86 eV can be inferred by linear extrapolation.

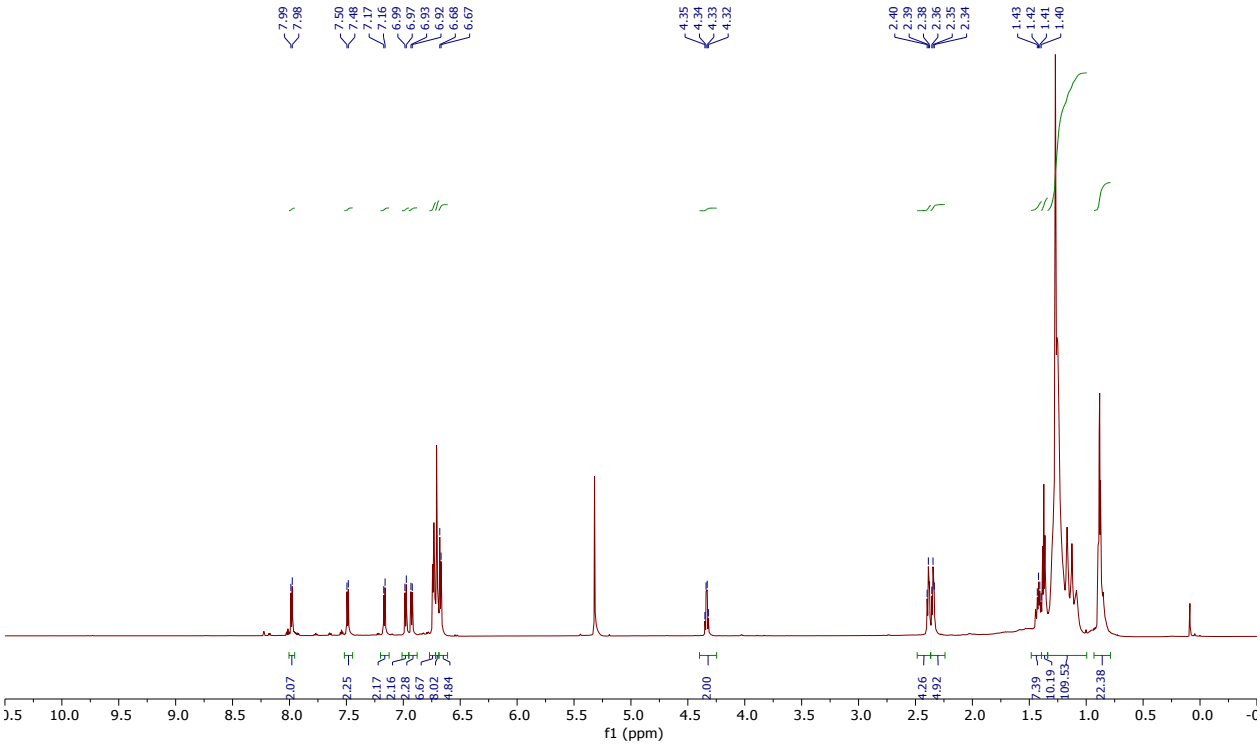

Figure S7. ^{1}H NMR spectrum of **2** in CD_2Cl_2 (700 MHz).

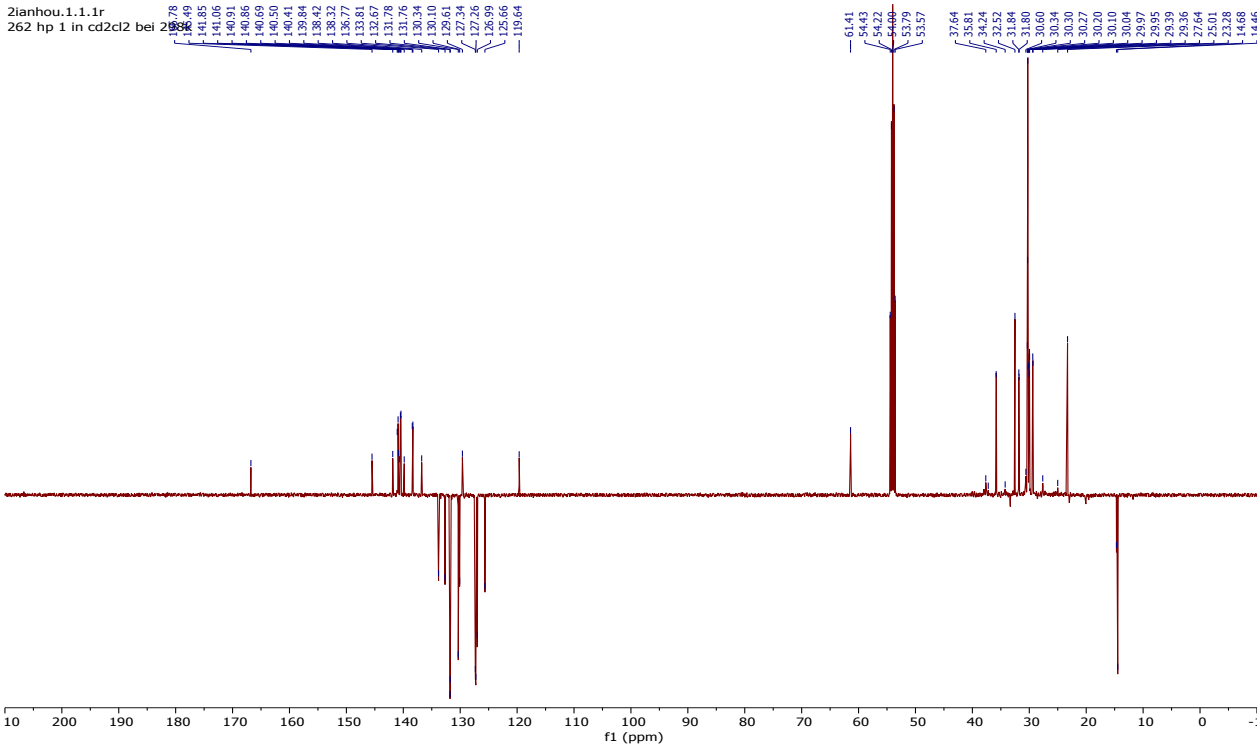

Figure S8. ^{13}C NMR spectrum of **2** in CD_2Cl_2 (126 MHz).

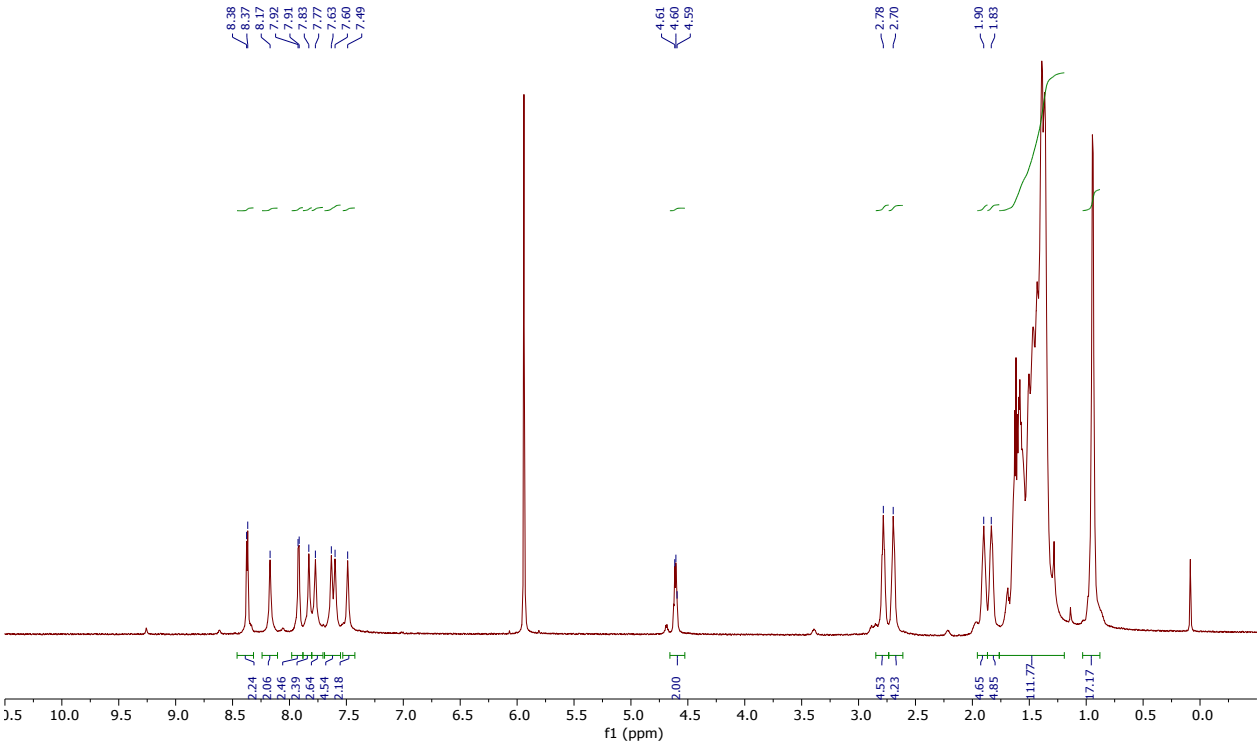

Figure S9. ^{1}H NMR spectrum of **3** in $C_2D_2Cl_4$ (700 MHz, 373 K).

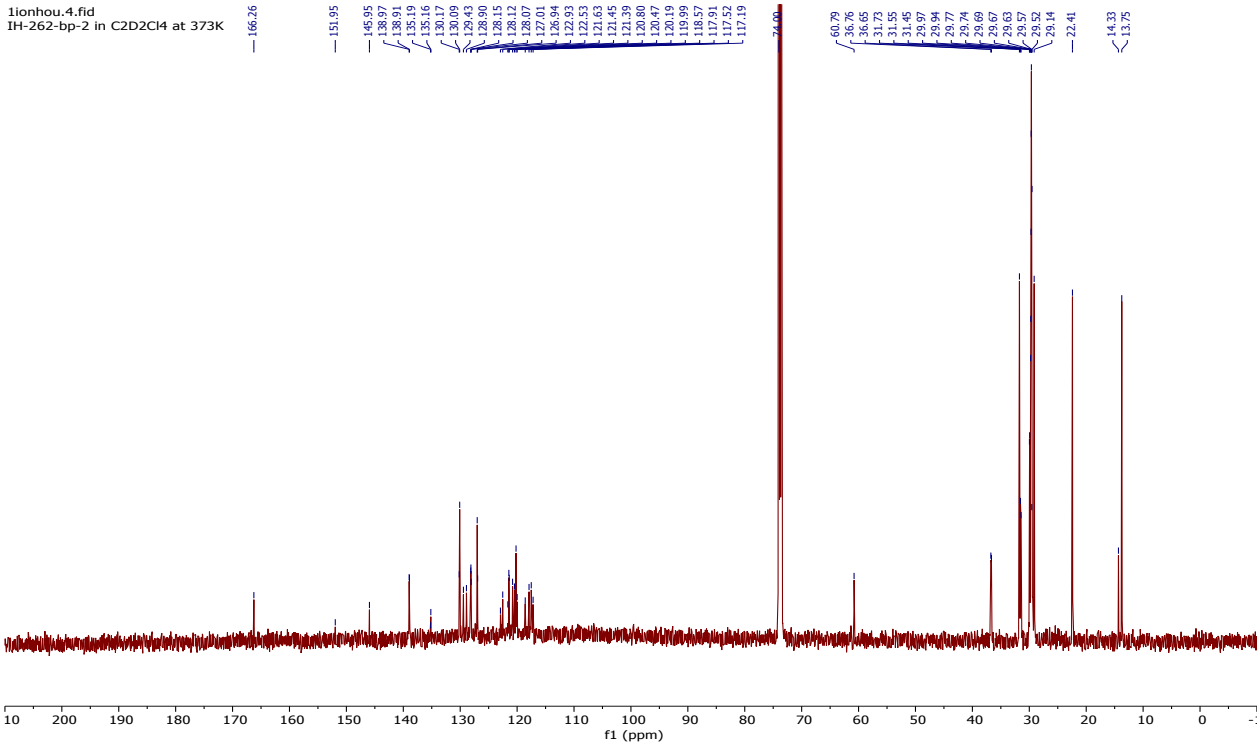

Figure S10. ^{13}C NMR spectrum of **3** in $C_2D_2Cl_4$ (176 MHz, 373 K).

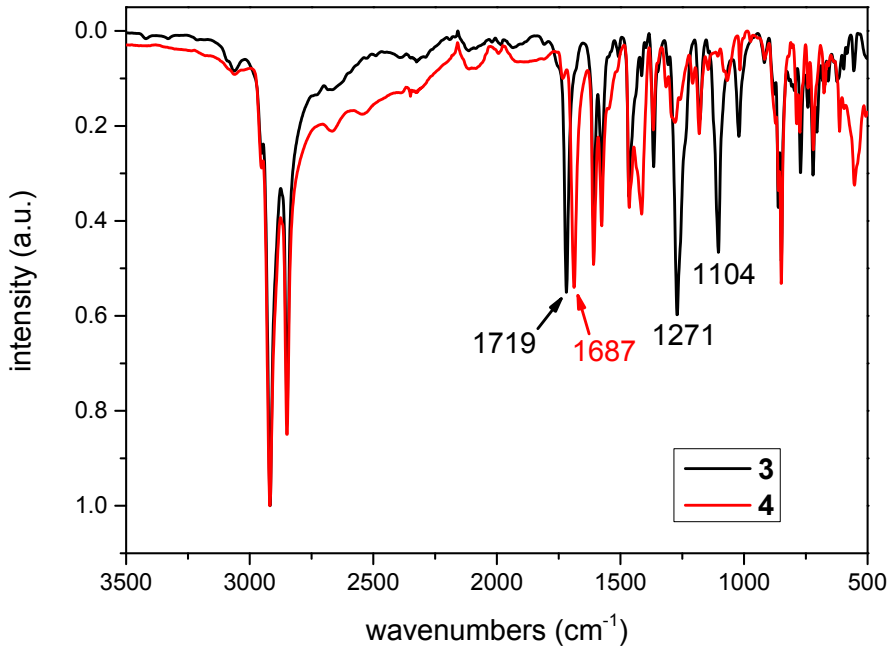

Figure S11. Infrared absorption spectra of **3** and **4**. The complete transformation of ester functional group into carboxylic group is clearly demonstrated by the infrared absorption spectral change of carbonyl functional groups, which shifts from 1719 cm^{-1} (benzoic ester) to 1687 cm^{-1} (benzoic acid).

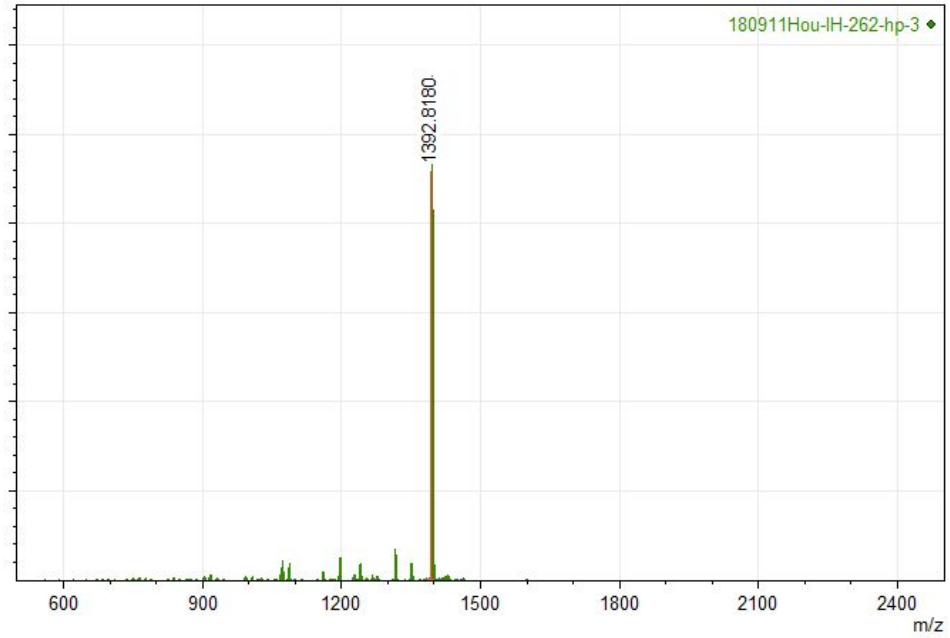

Figure S12. HRMS (MALDI-TOF) spectrum of **4** (matrix: TCNQ).

RERERENCES:

(1) Wang, H. I.; Lu, H.; Nagata, Y.; Bonn, M.; Cánovas, E. Dipolar Molecular Capping in Quantum Dot-Sensitized Oxides: Fermi Level Pinning Precludes Tuning Donor–Acceptor Energetics. *ACS Nano* **2017**, *11* (5), 4760–4767.

(2) Gaussian 09, Revision D.01, Frisch, M. J.; Trucks, G. W.; Schlegel, H. B.; Scuseria, G. E.; Robb, M. A.; Cheeseman, J. R.; Scalmani, G.; Barone, V.; Mennucci, B.; Petersson, G. A.; Nakatsuji, H.; Caricato, M.; Li, X.; Hratchian, H. P.; Izmaylov, A. F.; Bloino, J.; Zheng, G.; Sonnenberg, J. L.; Hada, M.; Ehara, M.; Toyota, K.; Fukuda, R.; Hasegawa, J.; Ishida, M.; Nakajima, T.; Honda, Y.; Kitao, O.; Nakai, H.; Vreven, T.; Montgomery, Jr., J. A.; Peralta, J. E.; Ogliaro, F.; Bearpark, M.; Heyd, J. J.; Brothers, E.; Kudin, K. N.; Staroverov, V. N.; Kobayashi, R.; Normand, J.; Raghavachari, K.; Rendell, A.; Burant, J. C.; Iyengar, S. S.; Tomasi, J.; Cossi, M.;Rega, N.; Millam, N. J.; Klene, M.; Knox, J. E.; Cross, J. B.; Bakken, V.; Adamo, C.; Jaramillo, J.; Gomperts, R.; Stratmann, R. E.; Yazyev, O.; Austin, A. J.; Cammi, R.; Pomelli, C.; Ochterski, J. W.; Martin, R. L.; Morokuma, K.; Zakrzewski, V. G.; Voth, G. A.; Salvador, P.; Dannenberg, J. J.; Dapprich, S.; Daniels, A. D.; Farkas, Ö.; Foresman, J. B.; Ortiz, J. V.; Cioslowski, J.; Fox, D. J. Gaussian, Inc., Wallingford CT, 2013.

(3) Baxter, J. B.; Schmuttenmaer, C. A. Conductivity of ZnO Nanowires, Nanoparticles, and Thin Films Using Time-Resolved Terahertz Spectroscopy. *J. Phys. Chem. B* **2006**, *110* (50), 25229-25239.

(4) Turner, G. M.; Beard, M. C.; Schmuttenmaer, C. A. Carrier Localization and Cooling in Dye-Sensitized Nanocrystalline Titanium Dioxide. *J. Phys. Chem. B* **2002**, *106* (45), 11716–11719.